Available online at www.sciencedirect.com
SCIENCE DIRECT®
Polymer 44 (2003) 3945–3961
polymer
www.elsevier.com/locate/polymer

Crystallization behavior of nylon 6 nanocomposites

T.D. Fornes, D.R. Paul*

Department of Chemical Engineering and Texas Materials Institute, University of Texas at Austin, Austin, TX 78712, USA

Received 6 January 2003; received in revised form 7 April 2003; accepted 10 April 2003

Abstract

The crystallization behavior of nylon 6 nanocomposites formed by melt processing was investigated. Nanocomposites were produced by extruding mixtures of organically modified montmorillonite and molten nylon 6 using a twin screw extruder. Isothermal and non-isothermal crystallization studies involving differential scanning calorimetry (DSC) were conducted on samples to understand how organoclay concentration and degree of clay platelet exfoliation influence the kinetics of polyamide crystallization. Very low levels of clay result in dramatic increases in crystallization kinetics relative to extruded pure polyamide. However, increasing the concentration of clay beyond these levels retards the rate of crystallization. For the pure nylon 6, the rate of crystallization decreases with increasing the molecular weight as expected; however, the largest enhancement in crystallization rate was observed for nanocomposites based on high molecular weight polyamides; this is believed to stem from a higher degree of platelet exfoliation in these nanocomposites. Wide angle X-ray diffraction (WAXD) and DSC were further used to characterize the polymer crystalline morphology of injection molded nanocomposites. The outer or skin layer of molded specimens was found to contain only γ-crystals; whereas, the central or core region contains both the α and γ-forms. The presence of clay enhanced the γ-structure in the skin; however, the clay has little effect on crystal structure in the core. Interestingly, higher levels of crystallinity were observed in the skin than in the core for the nanocomposites, while the opposite was true for the pure polyamides. In general, increasing the polymer matrix molecular weight resulted in a lower degree of crystallinity in molded samples as might be expected.

Keywords: Nanocomposites; Nylon 6; Crystallization

1. Introduction

The use of layered aluminosilicate as fillers in polymers has received considerable attention in recent years. Studies have repeatedly shown that dispersing individual high aspect ratio silicate platelets leads to dramatic property enhancements, e.g. increased stiffness and strength, improved barrier properties, and better dimensional stability at very low filler concentrations, often at a fraction of what is required for conventional fillers, such as talc or glass fibers. However, to date, well-exfoliated nanocomposites have been achieved for only a small number of polymer matrixes; this is governed, in part, by compatibility between the filler and matrix.

Organically modified layered silicates can be readily exfoliated in nylon 6 by either in situ polymerization or melt processing. The former technique, first demonstrated by Fujiwara and Sakamoto [1] and later optimized by Toyota researchers [2,3], consists of polymerizing ε-caprolactam in the presence of unmodified and organically modified montmorillonite, respectively. The technique of melt processing, proven viable by Christiani et al. [4], Lui et al. [5], and Cho et al. [6], involves compounding organically modified montmorillonite-nylon 6 mixtures in a twin screw extruder. More recent studies on nylon 6 nanocomposites have focused on how the organic modifier on the clay affects exfoliation and physical properties [7], how polymer chain tethering to the platelets influence nanocomposite morphology [8], how processing influences platelet exfoliation and orientation [9,10], how rheological behavior is altered by the exfoliated platelets [11–13], etc.

The effects of the silicate platelets on the crystal structure of the nylon 6 matrix of nanocomposites has also been of interest. Early investigations by Kojima et al. [14] and Liu et al. [5] suggest that the γ-crystalline form is enhanced by the addition of the clay, which is significant since crystalline structure may affect physical and mechanical properties. For

* Corresponding author. Tel.: +1-512-471-5392; fax: +1-512-471-0542.
E-mail address: drp@che.utexas.edu (D.R. Paul).

0032-3861/03/$ - see front matter © 2003 Elsevier Science Ltd. All rights reserved.
doi:10.1016/S0032-3861(03)00344-6

example, Ito et al. [15] showed that higher draw ratios of nylon 6 fibers can be achieved between 110 and 180 °C when the γ-crystalline form is present as compared to the α-form; specific details about the structure and properties of these two forms and a review of relevant investigations are given in the following section of this paper. Although many of the property enhancements seen in nylon 6 nanocomposites may be explained by the exfoliation and dispersion of high modulus, high aspect ratio platelets in a relatively low modulus matrix, some property effects [5,12,13] may be related to such crystalline modification of the polymer matrix. Therefore, it is important to understand, especially from a design standpoint, what factors influence the formation or enhancement of the crystalline forms of nylon 6 and how physical and mechanical properties may be affected.

The purpose of this paper is to examine the effects of organoclay concentration and degree of exfoliation on nylon 6 matrix crystal structure in nanocomposites formed by melt processing. A recent study involving three nylon 6 materials [12,13], varying in molecular weight, permits the comparison of nanocomposites having varying degrees of exfoliation. Emphasis will be placed on the isothermal and non-isothermal crystallization behavior of nylon 6 nanocomposites as well as crystalline properties of injection molded specimens. Differential scanning calorimetry (DSC) and wide angle X-ray diffraction (WAXD) are used to characterize the crystalline nature of the polyamide matrix in these nanocomposites. A detailed background section gives an overview of the different crystalline forms of nylon 6 and highlights past investigations relevant to this work.

2. Background

Aliphatic polyamides, such as nylon 6, are well known for their strong hydrogen bonding (H-bonding) ability and seek to maximize the number of H-bonds within and between polymer chains. All possible H-bonds are satisfied in the crystalline regions and a vast majority are consummated in the amorphous regions [16]. Furthermore, a sizeable fraction of H-bonds remain even in the molten state. These strong H-bonding characteristics dominate some physical behavior of polyamides like nylon 6.

Maximization of H-bonds in the crystalline state of nylon 6 requires the polyamide chains to adopt either a fully extended or twisted configuration. In the fully extended configuration, termed the α-form, polymer chains are oriented in an anti-parallel fashion, as shown in Fig. 1. Anti-parallel chains are situated such that the amide linkage and methylene units lie within the same plane, and the H-bonds occur between adjacent anti-parallel chains to form sheets of H-bonded chains. This structure repeats itself thereby creating stacks of H-bonded sheets in a monoclinic crystal. The γ-crystalline form of nylon 6 occurs, when H-bonds form between parallel polyamide chains. In this

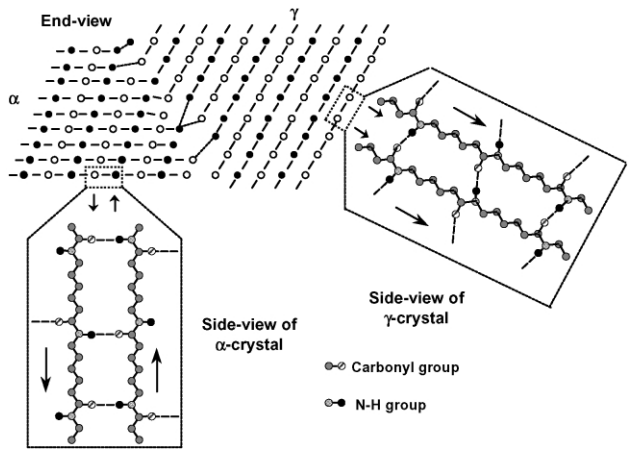

Fig. 1. Schematic of hydrogen bonding within the α and γ crystalline forms of nylon 6 as seen from end and side-view of each crystal. Closed and open circles represent chain axes projecting out of and into the page, respectively. Hydrogen bonds between polyamide chains are represented by dashed lines. The upper left hand portion of this figure was adopted from the work of Aharoni [16].

case, H-bond formation requires the amide linkages to twist approximately 60° out the plane of these molecular sheets otherwise only half of the possible H-bonds would be formed. Fig. 1 shows the side and end views of the γ-crystalline form of nylon 6. It is clear in these two views that the amide linkage no longer lies in the same plane as the CH_2 zigzags. Although the γ-form of nylon 6 was originally believed to be monoclinic [17], the chain packing more closely resembles that of a hexagonal structure and is referred to as pseudo-hexagonal.

Table 1 lists characteristic properties of the α- and γ-forms of nylon 6 [16–30]. The heats of fusion, $\Delta H_f°$, are the values reported by Illers [27]. It should be noted that other values for the α-form have been reported in the literature [23,27,29,31–35] and Wunderlich has suggested a value of 230 J/g based on a compromise of various reports in the literature [36].

The structure actually realized when nylon 6 is crystallized from the melt may be influenced by thermal conditions, applied stress, presences of moisture, and additives that are present. A concise overview of the influence of thermal conditions on crystal structure is given below. For a more complete synopsis of this and other aforementioned factors that affect the crystal structure of nylon 6, the reader is referred elsewhere [37].

The effect of crystallization temperature and time on the formation of the α versus γ-forms has been widely studied. For example, three independent investigations [28,38,39], have shown that crystallization for extend periods of time below ~130 °C leads solely to the γ-crystallites while above ~190 °C only the α-form is produced. Temperatures in between these limits result in a mixture of the two forms, with higher fractions of α produced at higher temperatures. The disappearance of the γ-form at ~190 °C has been commonly referred to as the Brill transition, a phenomenon

Table 1
Miscellaneous data for the α and γ crystalline forms of nylon 6

Property	α	γ	Reference(s)
Crystal structure	Monoclinic	Hexagonal/pseudohexagonal	
Lattice constants	$a = 0.956$ nm $b = 1.724$ nm (fiber axis) $c = 0.801$ nm $\beta = 67.5°$	$a = 0.472$ nm[a] $c = 1.688$ nm[a] $\gamma = 120°$[a]	[17–19]
Crystallographic reflection(s)	(200) (002/202)	(001) (200/20$\bar{1}$)-minor	[16,18,20]
Characteristic d-spacings	$d_{200} \cong 0.370$ nm $d_{002+202} \cong 0.440$ nm	$d_{001} \cong 0.413$ nm	[16,18,21,22]
Density, ρ (g/cm^3)	1.23 (experimental) 1.23 (calculated)	1.16–1.19 (experimental) 1.16 (calculated)	[18,21,23–30], amorphous $\rho = 1.09$
Heat of fusion, $\Delta H_f°$ (J/g)	241	239	[27]

[a] Hexagonal lattice constants were calculated based on the monoclinic parameters $a = 0.933$ nm, $b = 1.688$ nm, and $c = 0.478$ nm and $\beta = 121°$. The hexagonal lattice constant, a, was taken as the average of a and half of b of the monoclinic unit cell. The constant c representing the fiber axis remained fixed.

first observed in nylon 6,6 [40]. This transition corresponds to the merging of the two reflections of the α-form into a single peak in plots of X-ray diffraction intensity versus 2θ [41–44] as the sample is heated. Kyotani and Mitsuhashi [39] also found that very short crystallization times at either 100 or 200 °C lead to both crystalline forms, while longer times produced predominantly γ and α, respectively. In general, rapid cooling or quenching from the melt produces the γ-form [41,45–47]. Annealing also affects the crystal structure. For example, annealing of quenched samples, or those crystallized between 100 and 150 °C, at 200 °C for extended times leads to the conversion of the γ into α [39]. Similar annealing results were demonstrated by Gogolewki et al. [29] and Gurato et al. [38].

Based on the above, it is clear that, in general, rapid cooling and low temperature crystallization promotes the γ-form of nylon 6, while higher crystallization temperatures or slow cooling leads to the α-form. Kyotani and Mitsuhashi [39] attribute the temperature dependence to the crystallization rates of the two forms; i.e. at temperatures below 130 °C the rate of formation of γ is faster, while above ~190 °C the crystallization rate of α is faster, while at intermediate temperatures, the rates are comparable. Interestingly, the maximization crystallization rate of nylon 6 occurs at approximately 140 °C [48]. The temperature dependence of the crystallization rate above this maximum is dominated by the driving force for crystallization, i.e. the degree of undercooling, while below, the rate is dominated by the resistance to crystallization, i.e. polymer chain mobility. Therefore, it may be postulated that conditions of limited polymer chain mobility favor the crystallization of the γ-form for nylon 6.

Studies of nylon 6-based nanocomposites have caused renewed interest in the factors affecting the crystalline structure. As mentioned above, Kojima et al. [14] and Liu et al. [5] reported that when the one nanometer thick platelets of montmorillonite are dispersed in nylon 6 the polymer crystallizes in the γ-form. The higher level of γ-form observed in the Toyota study, however, could be influenced by the high shear and rapid cooling inherent to injection molding, since the pure polyamide was also predominantly of the γ-form. Details of the thermal and processing history in the study by Liu et al. [5] were not specified. The latter authors state that the clay acts as a strong heterogeneous nucleating agent, capable of increasing crystallization temperatures in comparison to pure nylon 6 as shown by DSC cooling scans. A number of more detailed investigations that better address the role of dispersed silicates on nylon 6 crystalline structure have appeared recently.

Wu and coworkers [49–52] examined the influence of thermal treatment on the crystallization behavior of melt processed nanocomposites using FTIR, WAXD, and DSC. From FTIR measurements on thin film samples, it has been claimed that the hydrogen bonding in both crystalline forms of nylon 6 is weakened by the presence of the clay. WAXD analysis revealed that nanocomposites films exhibit both crystalline forms when slowly cooled from the melt; whereas, pure nylon 6 gave predominantly the α form. Methods that permit higher cooling rates, e.g. air and water-cooling, increased the content of the γ-phase especially for the nanocomposite. Further WAXD investigations conducted on samples that had been annealed at different temperatures showed the onset of the γ to α transition, normally observed around 130 °C for pure nylon 6, in this case 120 °C, occurred approximately 40 °C higher for the nanocomposite. Interestingly, an unexpected higher amount of γ-form was observed after annealing at 200 °C than at 180 °C. Lastly, non-isothermal crystallization surprisingly showed that the degree of crystallinity increased with increasing cooling rate for the nanocomposites, counter to what is observed in pure nylon 6 and other polymers. It should be noted that in this work an epoxy material was intercalated into the organoclay melt prior to mixing with nylon 6. It is unclear what effect the epoxy has since results without this material were not reported.

Wu and Liao examined the effect of thermal history and filler concentration on the crystal structure of nylon 6 nanocomposites formed by in situ polymerization using synthetic saponite and natural montmorillonite [53,54]. Similar crystalline behavior was observed for the pure and nanocomposite materials when samples were slowly or rapidly cooled from the melt; however, nanocomposites containing a low concentration of saponite, i.e. 2.5 wt%, favored the formation of the α-form regardless of the cooling conditions. Annealing studies showed that higher amounts of γ were present in the nanocomposite than in pure nylon 6 after annealing at high temperatures, except at low saponite contents.

Some studies have explored the differences between nylon 6 nanocomposites formed by in situ polymerization and by melt processing. Based on DSC and solid state NMR studies, VanderHart et al. [55,56] concluded that the silicate layers promote the γ-form regardless of the formation technique, and that γ-crystallites reside near the polyamide/clay interface. Lincoln et al. [8] used small angle X-ray scattering, in addition to WAXD and DSC, to infer about the crystalline morphology of these two types of nanocomposites. They concluded that the clay platelets disrupt the formation of crystallites and the extent of platelet-crystallite interactions is dependent upon the technique used to form the nanocomposites. In other words, the nature of the bond between the clay and polyamide chains seems to influence clay–crystallite interactions.

3. Experimental

3.1. Materials

Three commercial grades of nylon 6 from Honeywell, with high, medium, and low molecular weights (M_n = 29,300, 22,000, 16,400), referred to here as HMW, MMW, and LMW, respectively, were used to form nanocomposites as described previously [12,13]. Organoclay from Southern Clay Products was produced by cation exchange between sodium montmorillonite (CEC = 92 meq/100 g clay) and bis(hydroxyethyl)-(methyl)-rapeseed quaternary ammonium chloride, designated as $(HE)_2M_1R_1$; rapeseed is a natural product consisting of predominantly unsaturated C_{22} alkyl chains.

3.2. Melt processing

Melt blended nanocomposites were formed using a Haake co-rotating twin screw extruder with the barrel temperature set at 240 °C, a screw speed of 280 rpm, and a feed rate of 980 g/hr as described previously [12,13]. The amount of montmorillonite (MMT) in each extrusion batch was determined by placing pre-dried nanocomposite pellets in a furnace at 900 °C for 45 min and weighing the remaining MMT ash. A correction for loss of structural water in the clay is made in the calculation [12,13].

Extruded nanocomposites pellets were dried and then injection molded into standard Izod bars (ASTM D256, Type I) in an Arburg Allrounder 305-210-700 injection molding machine using a barrel temperature of 260 °C, mold temperature of 80 °C, injection pressure of 70 bar, and a holding pressure of 35 bar.

3.3. Differential scanning calorimetry (DSC)

Isothermal crystallization behavior of the nylon 6 and its nanocomposites was determined using a Perkin–Elmer DSC 7. The specimens were excised from extruded strands that were quenched in water, air dried, and pelletized. The resulting pellets were dried under vacuum for approximately 12 h at 80 °C prior to the thermal analysis. Samples were heated from 25 to 250 °C at 20 °C/min, held for 1 min to ensure melting, then rapidly cooled to 197 °C where they were allowed to crystallize for 65 min. The chosen crystallization temperature of 197 °C was determined through a series of experiments conducted at various crystallization temperatures. Below 197 °C onset of crystallization for the low LMW polyamide overlapped with the initial transient portion of heat flow curve. Setting T_c = 197 °C eliminated this problem for the nanocomposites based on LMW nylon 6, while allowing completion of crystallization in reasonable lengths of times for the HMW-based materials. Isothermal experiments were also conducted on both as-received pellets and extruded versions of the pure nylon 6 materials for comparative purposes. These samples were dried prior to testing under the same conditions as mentioned above.

In addition, non-isothermal behavior was followed using heating and cooling scans for specimens taken from extruded pellets, as described above, and injection molded bars. Injection molded samples were taken from dry as-molded 3.18 mm thick Izod bars at depths from the surface of 0.2 and 1.5 mm, corresponding to the skin and core regions, and directly analyzed. All samples were held at −10 °C for 2 min, heated at a rate of 20 °C/min to 250 °C and subsequently held for 1 min, then cooled at a rate of 20 °C/min to −10 °C. Specimens from extruded pellets were heated again to assess the effects of the previous cooling scan. Heating scans were analyzed for the glass transition temperature, T_g, melting temperature, T_m, heat of fusion, ΔH_f, while cooling scans were used to obtain the crystallization temperature, T_{cc}. In some cases, the lack of any inflection in the heating curve prevented determination of T_g. The heat of fusion, which was determined by integrating the heat flow from 150 to 250 °C, was used to calculate the level of crystallinity, defined by the ratio of ΔH_f to the heat of fusion of the purely crystalline forms of nylon 6, as indicated in Table 1. Since the ΔH°_f values of both crystalline forms of nylon 6 are nearly identical, the level of crystallinity was calculated using the average of the

two, i.e. 240 J/g. Heats of crystallization, ΔH_c, were determined by integrating cooling scans from 100 to 200 °C. Fig. 2(a) shows a representative example of a full heating and cooling cycle and the integration technique used to calculate ΔH_f and ΔH_c.

3.4. Wide angle X-ray diffraction (WAXD)

WAXD was conducted using a Sintag XDS 2000 diffractomer in the reflection mode using an incident X-ray wavelength of 1.542 Å at a scan rate of 1.0°/min. X-ray analysis was performed at room temperature on milled (i.e. top 1.02 mm removed) and pristine Izod bars. The Izod specimens were oriented such that the incident beam reflected off the major face, as described in a previous study [12,13]. The resulting plots of X-ray intensity versus 2θ were analyzed using the profile fitting program PeakFit™ (AISN Software Inc.). The 2θ locations of the α- and γ-crystalline forms were identified by peak intensities occurring at approximately $2\theta = 20$ and 23.7° for the α-form, i.e. α_1 and α_2, and 21.3° for the γ-form. The peak locations in 2θ were held constant, while the peak heights and widths were allowed to vary. The amorphous peak location was allowed to float, but was generally located at $2\theta = 21.43° \pm 0.01$. Prior to executing the auto-fit program, the height and breadths of each peak were adjusted manually in order to provide a reasonable starting point for the curve fitting algorithm to begin. Each peak was modeled using a Gaussian—Lorentzian peak shape. Areas of the peaks obtained from the analysis were used to estimate the degree of crystallinity for each phase, i.e. the ratio of the areas of the crystalline reflections to that of total area of the scattering curve (amorphous + crystalline). In general, agreement between model predictions and the data were exceptional, yielding coefficients of determination, i.e. R^2, above 0.98. Despite the good agreement, the degree of crystallinity obtained via this analysis should be treated as approximate, since the initial guess for each peak will influence these results. The uncertainty estimated for the crystallinity values is on the order of 10–20% of the mean. Higher uncertainty is expected for samples that contain multiple crystalline forms. Fig. 2(b) is a representative example of a diffraction curve that has been resolved into crystalline and amorphous scattering components using the peaking fitting software.

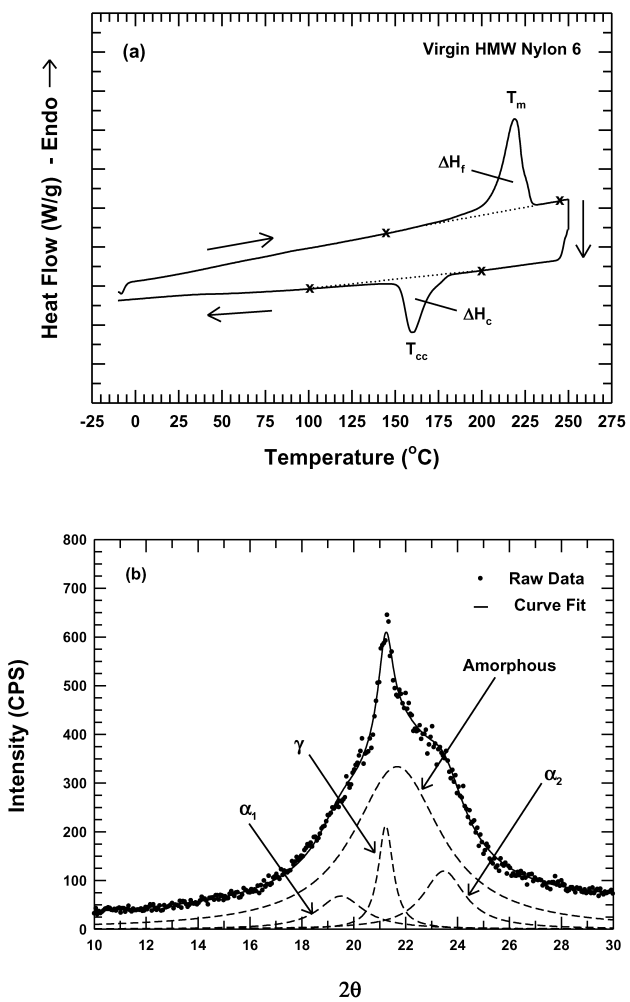

Fig. 2. Representative examples of (a) a complete DSC heating and cooling scan and the analytical technique used to determine ΔH_f, T_m, ΔH_c, and T_{cc} and (b) a WAXD pattern (pure MMW injection molded specimen—core scan) and the profile fitting technique used to deconvolute the amorphous and crystalline phases.

4. Results and discussion

Previous work conducted in this laboratory showed that high molecular grades of nylon 6 lead to better exfoliation of clay platelets owing to the higher levels of shear stresses in the extruder caused by the higher melt viscosity. This series of nanocomposites [12,13] offer an excellent opportunity to better understand how polyamide matrix molecular weight, clay concentration, and the level of clay platelet exfoliation affect polyamide crystalline morphology; understanding such effects is especially important since the resulting crystalline structure will ultimately influence nanocomposite physical and mechanical properties. Elucidation of these issues is also vital with regard to the design and fabrication of commercial nanocomposites via different processes, e.g. injection molding, blow molding, film extrusion, etc. Therefore, it is our intent to examine how the above factors influence the crystalline structure of nylon 6 nanocomposites formed by melt processing. Thermal and processing history also alter crystal structure as mentioned previously in the background section; thus, results pertaining to specific DSC and WAXD analyses of injection molded specimens are discussed.

4.1. Isothermal crystallization of nylon 6 nanocomposites

An extensive analysis of isothermal crystallization

behavior was carried out on pure nylon 6 and its nanocomposites. To rightfully compare pure nylon 6 materials with its nanocomposites, it was necessary to extrude the pure polyamides under the same processing conditions used to form the nanocomposites. Fig. 3 shows the isothermal crystallization behavior of virgin, i.e. from as-received pellets, and extruded nylon 6 materials. Regardless of the molecular weight, the extruded materials exhibit faster crystallization than the virgin samples. There are several possible reasons why such behavior is observed. Faster crystallization may arise from increased nucleation due to the presence of impurities incorporated in the matrix during processing. Memory effects associated with thermal and stress histories that remain present in the sample after annealing in the melt may also lead to an increased rate of crystallization. Numerous studies have shown that the processing history of the polymer, e.g. melting, mixing, cooling, pelletizing, etc. are often not fully erased when the polymer is annealed at high melt temperatures [16,57–62]. Aharoni reports that any shearing imposed on the polymer during melt processing may facilitate the production of aligned arrays of H-bonded sections that act as stable nuclei, capable of remaining intact in the melt state for long periods of time [16]. These arrays ultimately act as crystallization sites upon cooling from the melt. Indeed, Khanna et al. showed that extruded nylon 6 leads to faster crystallization than virgin nylon 6 under both isothermal and non-isothermal conditions [58]. The temperature of melting and the length of time held in the molten state will also determine the amount of stable nuclei remaining prior to recrystallization; this issue has been the topic of many investigations [62–67]. For example, Avramova and Fakirov showed that onset time of crystallization occurred at significantly shorter times for nylon 6 samples annealed below 280 °C for extended periods of time than samples annealed above this temperature [67]. In addition to impurities and memory effects, generation of low molecular weight chains during processing, i.e. through degradation [68], may facilitate increased polymer chain mobility and lead to faster crystallization.

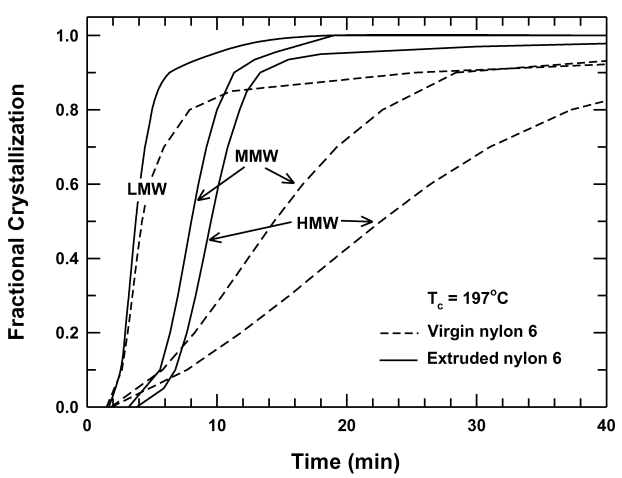

Fig. 3. Fractional crystallization curves obtained at 197 °C via DSC for samples taken from virgin and extruded nylon 6 materials. Samples were obtained from pellets that were dried under vacuum for 12 h at 80 °C prior to DSC analysis. Fractional crystallization represents the fraction of crystallizable polymer that has been crystallized at given time.

The above demonstrates that processing alone significantly affects the crystallization behavior of nylon 6; therefore, for proper comparison between pure nylon 6 and the nanocomposites, the 0 wt% MMT data presented in the remaining plots represent the extruded version of nylon 6. Fig. 4 shows the dependence of heat flow on crystallization time at 197 °C for different loadings of clay in each of the three nylon 6 nanocomposites. Addition of small amounts of organoclay to each polyamide matrix results in a significant reduction in crystallization time; however, further addition of clay reverses this trend which is most obvious in the LMW system, as seen in Fig. 4(a). At levels of 1.6 wt% MMT and beyond, the peak location of each exotherm occurs at times comparable to, and in some cases longer, than the pure extruded polyamide. Similar behavior is observed in the MMW and HMW systems as well (See Fig. 4(b) and (c)).

The kinetics of crystallization may be better visualized by plotting fractional crystallization versus time, as seen in Fig. 5. These curves reiterate that very small amounts of clay dramatically increase the rate of crystallization; however, high clay concentrations reduce the rate of crystallization. In some cases, the crystallization of the nanocomposites is slower than the pure extruded polyamide. Similar effects have been observed for nanocomposites in other matrices like poly(ε-caprolactone) systems [69]. The clay particles serve as additional nucleation sites; however, high clay contents clearly retard the growth process. At low concentration of clay, the distance between dispersed platelets is large so it is relatively easy for the additional nucleation sites to incorporate surrounding polymer. However, at high concentrations of clay, diffusion of polymer chains to the growing crystallite is hindered. The combination of a larger number of nucleation sites and limited crystal growth is expected to produce crystals of fine grain size. Indeed, Ma et al. showed by polarized optical microscopy that addition of organoclay increased the number and decreased the size of spherulites formed in polypropylene [70]. In accord with this, the nanocomposites materials described here were more transparent than the virgin polyamide in the form of thin injection molded specimens.

In general, decreasing the polyamide molecular weight results in faster crystallization, as seen in Figs. 3–5. This is to be expected on the basis of mobility considerations and has been observed for many polymers as summarized by Wunderlich [71]. A concise picture of the effects of matrix molecular weight on the crystallization kinetics for nylon 6 nanocomposites can be seen from plots of time of half-crystallization, $t_{1/2}$, versus clay concentration. Fig. 6(a) shows a plot of $t_{1/2}$ versus silicate concentration for the

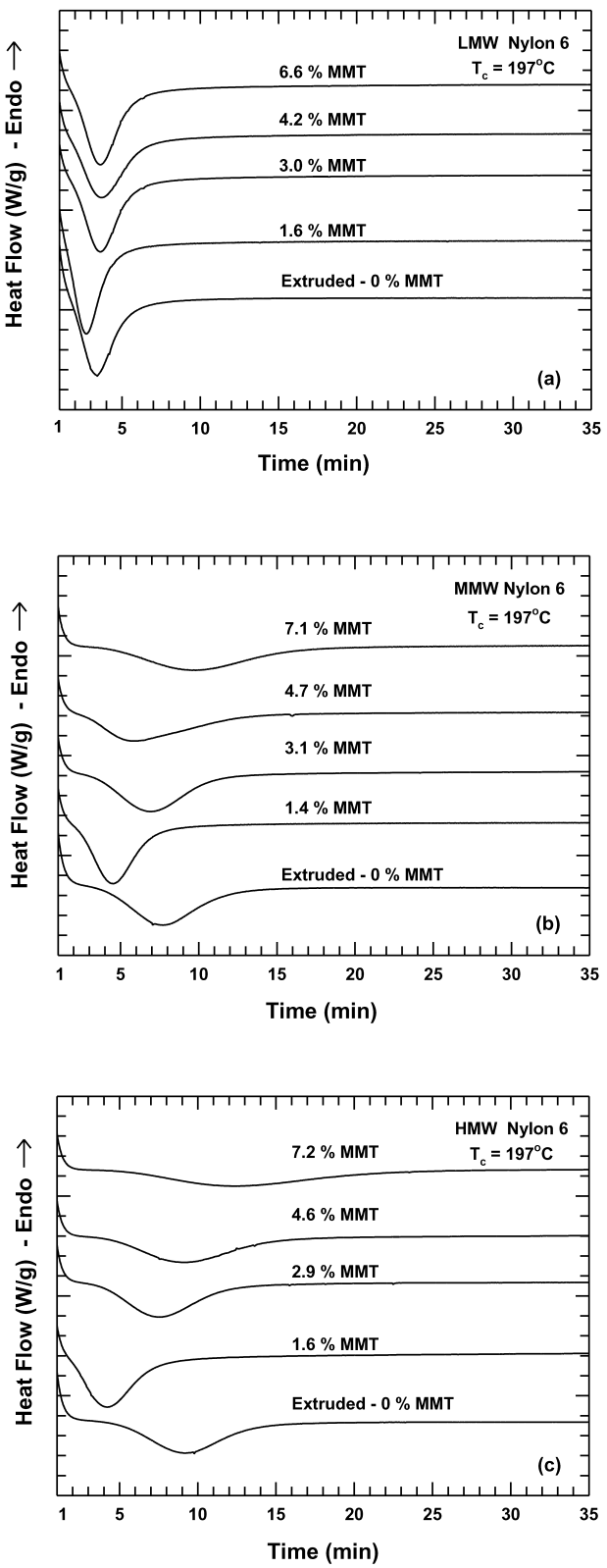

Fig. 4. Crystallization isotherms obtained at 197 °C via DSC for samples taken from extruded nylon 6 and its nanocomposites based (a) LMW, (b) MMW, and (c) HMW nylon 6. Samples were obtained from pellets that were dried under vacuum for 12 h at 80 °C prior to DSC analysis. Scans are shifted for clarity.

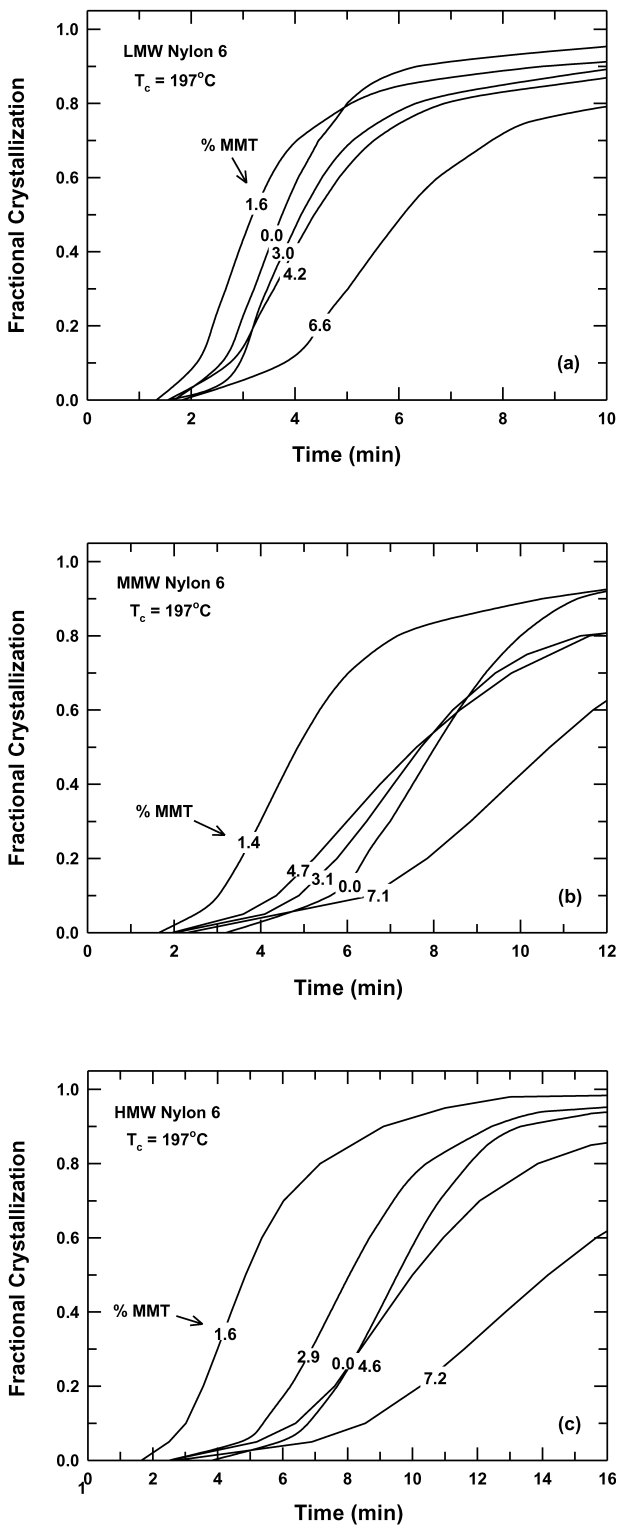

Fig. 5. Fractional crystallization curves for extruded nylon 6 and its nanocomposite samples based (a) LMW, (b) MMW, and (c) HMW nylon 6.

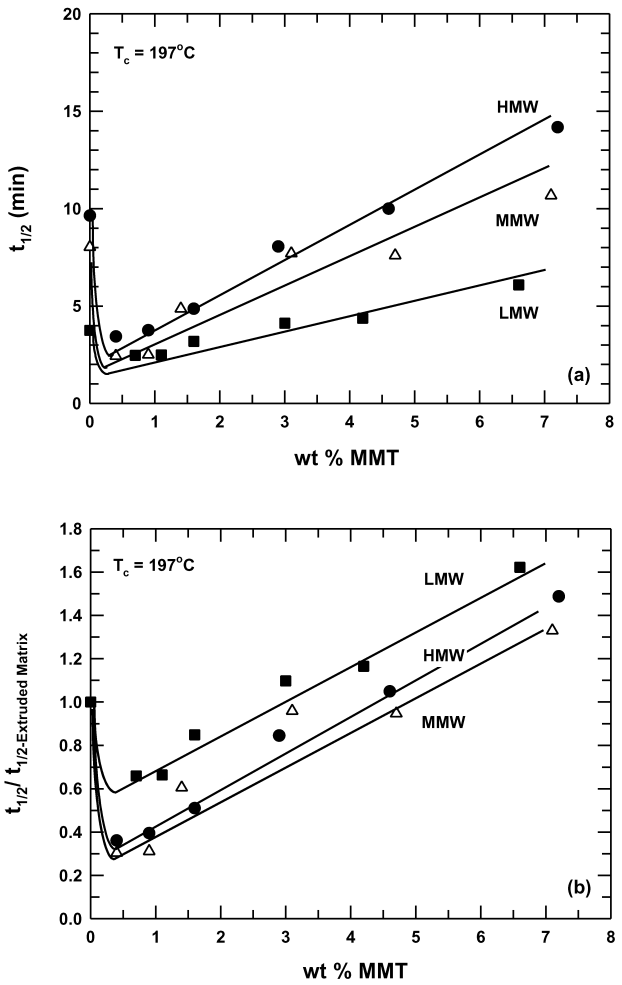

Fig. 6. The effect of clay concentration (inorganic) on the (a) half time of crystallization, $t_{1/2}$, and (b) half time of crystallization normalized to the each extruded matrix for nanocomposites based on LMW, MMW, and HMW nylon 6. The 0 wt% MMT data points represent extruded versions of nylon 6.

nanocomposites formed using the three different polyamide matrices. Adding small amounts of clay to each matrix, i.e. nominally 0.5 wt% MMT, results in a sizeable reduction in half time; however, beyond this concentration the clay actually retards crystallization. Furthermore, the crystallization kinetics is comparable to the extruded matrices at commercially relevant concentrations, i.e. 3–5 wt% MMT. Interestingly, several studies involving a variety of nucleating agents, including talc which is a member of the layered aluminosilicate family, have shown that the maximum crystallization rate of nylon 6 occurs at additive concentrations in the range ~0.1–0.5 wt% [34,71–73]. What is surprising in Fig. 6(a) is the large relative decrease in crystallization time observed in the higher molecular weight matrices. Adding low concentrations of MMT to high molecular weight matrices leads to more than a 63% decrease in $t_{1/2}$; whereas, the LMW nanocomposites exhibit only a 34% decrease relative to the extruded polyamide. Rightful comparison of these kinetic effects require normalization of nanocomposite half times with respect to those of the polyamide matrices, as shown in Fig. 6(b). This plot shows that higher molecular weights are more effective for increasing the kinetics of nylon 6 crystallization. This trend is believed to stem from the increased levels of clay platelet exfoliation, which provides more sites for nucleation and subsequent crystal growth. Interestingly, a study on the influence of nucleating agents on the isothermal crystallization of nylon 6 by Gurato et al. [72] showed that smaller talc particles are more effective in lowering half times of crystallization than larger ones; this may be associated with increased number of particles or amounts of surface area on which crystals are able to originate and grow. In the case of MMT, exfoliation of thin 1 nm thick individual layers or sheets leads to dramatic increases in filler surface area; this is expected to significantly alter the crystallization process. The higher exfoliation levels previously seen for the high molecular weight nylon 6 [7,12,13] and the lower relative half times reported here support this hypothesis.

Fractional crystallization curves like those in Fig. 5 can also be analyzed in terms of the Avrami equation [71,74–76], often used to describe the initial stage of crystallization, i.e., primary crystallization,

$$1 - X(t) = \exp(-Kt^n) \tag{1}$$

where $X(t)$ is the fraction of crystallizable polymer that has been crystallized at time t, n is a parameter that describes the nucleation and growth process, and K is the crystallization rate constant. The parameters n and K were obtained by fitting isothermal crystallization data at $X(t) < 0.5$ to a linearized form of the Avrami equation.

$$\ln[1 - \ln(1 - X(t))] = \ln K + n \ln t \tag{2}$$

Linear regression was used to obtain n and K, see Table 2, from plots of the data in the form suggested by Eq. (2). The values of n for the virgin, as received, polyamides range from 1.75 to 4.17 and are consistent with values reported in literature [64,71,77,78]; however, values of n for the extruded versions of these materials are much higher and vary little with molecular weight as also shown by Khanna et al. [58]. The increase in n is likely a reflection of memory effects associated with the processing of the polyamides, as mentioned above.

The addition of exfoliated silicate platelets in each matrix results in significant changes in the Avrami constants relative to the extruded nylon 6 materials, as shown in Fig. 7(a) and (b). In general, n shows a gradual decrease with increasing MMT content; whereas, the primary crystallization rate constant K, shows a maximum at the lowest MMT concentrations. Values of n for neat nylon 6 are indicative of the growth of sheaf-like crystallites, but adding clay, causes n to approach a value of four which is consistent with spherical growth [71]. It should be noted that the absolute values of n for the nanocomposites are in accord with the values reported by Gurato et al. [59] for nylon 6—talc composites. The trend in K reiterates that adding small

Table 2
Kinetic analysis of isothermal crystallization data obtained on extruded pellets of nylon 6 nanocomposites based on $(HE)_2M_1R_1$ organoclay

Polymer sample	% MMT	ΔH_c (J/g)	$t_{1/2}$ (min)	Avrami constants	
				n	$K \times 10^4$ (min^{-n})
LMW-virgin[a]	0.0	86.1	4.2	4.2	18.0
MMW-virgin[a]	0.0	74.8	14.4	2.1	27.6
HMW-virgin[a]	0.0	71.9	22.6	1.8	129
LMW-extruded	0.0	60.9	3.8	5.1	18.0
LMW	0.7	61.2	2.5	4.7	121
LMW	1.1	53.2	2.5	4.7	110
LMW	1.6	67.0	3.2	4.6	37.5
LMW	3.0	71.5	4.1	4.5	12.1
LMW	4.6	70.2	4.4	4.3	14.5
LMW	6.6	71.4	6.1	4.0	5.44
MMW-extruded	0.0	58.0	8.0	5.3	0.12
MMW	0.4	66.3	2.4	5.0	100
MMW	0.9	66.5	2.5	4.3	171
MMW	1.4	69.9	4.9	4.2	10.8
MMW	3.1	73.9	7.7	4.2	1.51
MMW	4.7	65.2	7.6	4.1	2.53
MMW	7.1	66.4	10.7	3.9	0.73
HMW-extruded	0.0	53.9	9.5	5.6	0.03
HMW	0.4	63.3	3.4	5.4	9.64
HMW	0.9	58.9	3.4	5.0	16.3
HMW	1.6	63.7	4.9	4.6	6.23
HMW	2.9	57.6	8.1	4.5	0.64
HMW	4.6	59.9	10.0	4.3	0.39
HMW	7.2	58.1	14.2	3.7	0.36

[a] Virgin samples were obtained from as-received nylon 6 pellets.

amounts of clay leads to the most dramatic increase in crystallization kinetics, while larger amounts impedes the process.

4.2. Non-isothermal crystallization of nylon 6 nanocomposites

Non-isothermal crystallization studies were carried out by heating to 250 °C and holding for 1 min prior to cooling at 20 °C/min. Fig. 8 compares DSC cooling scans for the virgin and extruded versions of the nylon 6 materials. The extruded polyamide has higher crystallization temperatures and narrower peak widths than the as received, virgin samples, regardless of the matrix molecular weight. These results are very similar to the differences observed in the isothermal studies. The higher crystallization temperatures result from increased crystallization rates believed to arise from thermal and stress histories that remain after melting. Evidence of such effects have been reported by Khanna et al. [57–61] and Aharoni et al. [16]; Aharoni et al. investigated the influence of melt anneal temperature on the crystallization temperature of unground and finely ground pellets of nylon 6 under non-isothermal conditions. The crystallization temperature decreased with increasing annealing temperatures, indicating some destruction of

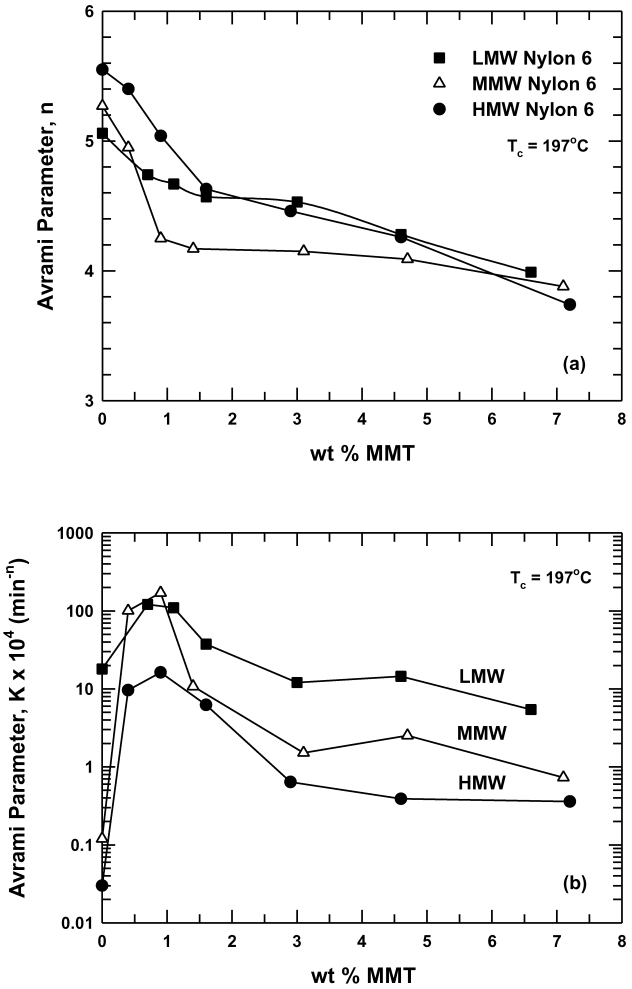

Fig. 7. The effect of clay concentration (inorganic) on the Avrami parameters (a) n and (b) K for nanocomposites based on LMW, MMW, and HMW nylon 6. The 0 wt% MMT data points represent extruded versions of nylon 6.

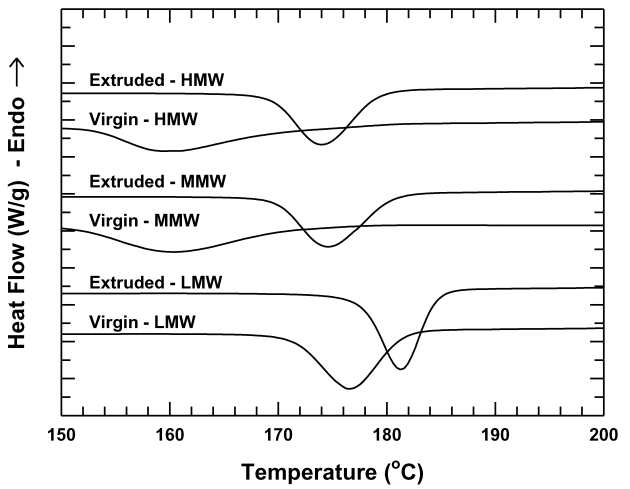

Fig. 8. Cooling scans of samples taken from pellets of virgin and extruded LMW, MMW, and HMW nylon 6 materials. Samples were obtained from pellets that were dried under vacuum for 12 h at 80 °C prior to DSC analysis. Samples were held at 250 °C for 1 min prior to cooling at 20 °C/min. Scans are shifted for clarity.

stable crystallites. However, the crystallization temperature for the finely ground samples remained much higher than the unground pellets even at the highest annealing temperature, i.e. 290 °C. Similar memory effects are believed to exist in the present nanocomposite system. Lastly, the increase in crystallization temperature with decreasing molecular weight of the nylon 6 seen in Fig. 8 is a result of increased chain mobility; this phenomenon is well known in the literature, as summarized by Wunderlich [71].

Fig. 9 shows the cooling scans for the extruded nylon 6 and the nanocomposites. Similar conclusions as those made in the previous section may be drawn with regard to the effects of clay concentration and polyamide molecular weight. Each graph illustrates that adding intermediate to high levels of clay actually decreases the crystallization temperature, T_{cc}. As mentioned above, introducing more particles hinders chain mobility and, thus, retards crystal growth. As seen in Fig. 9, increasing the matrix molecular weight, in all cases, results in lower T_{cc} values and smaller heats of crystallization, ΔH_c. Further evidence of slower kinetics for the MMW and HMW based materials can be seen in the x_c values obtained upon subsequent heating (see second heating, Table 3). As mentioned above, the trend in molecular weight arises from differences in polymer chain mobility.

4.3. Polyamide crystal structure of injection molded nanocomposites

Injection molding is a very common method for fabricating thermoplastic parts. The key step in this operation is the injection of the polymer melt under high pressures into a mold or cavity, which is cooled well below the melting point of the polymer causing the polymer to freeze, thereby resulting in a solid part of desired shape. The temperature at which the mold is kept is an important process variable, particularly for semi-crystalline polymers, since it governs heat transfer between the polymer and mold and will ultimately control the crystallization process; consequently, mold temperature affects physical and mechanical properties of the molded part. In addition to heat transfer, the shear stresses imposed on the polymer melt caused by rapid injection is an important factor in the crystallization process. High degrees of stress, particularly at the mold surface, causes polymer chains to align in the direction of flow, thereby facilitating crystallization. Generally the outer-most layer undergoes rapid cooling, while the central portion of the molded part experiences slower cooling rates and less stress; this produces a skin-core structure due to the differences in cooling and chain orientation [79]. Differences in the physical and mechanical properties between the core and skin can be significant. In glass fiber-reinforced semicrystalline thermoplastics reinforced, the skin and core differ in both the crystallization and orientation of the polymer matrix and in the orientation

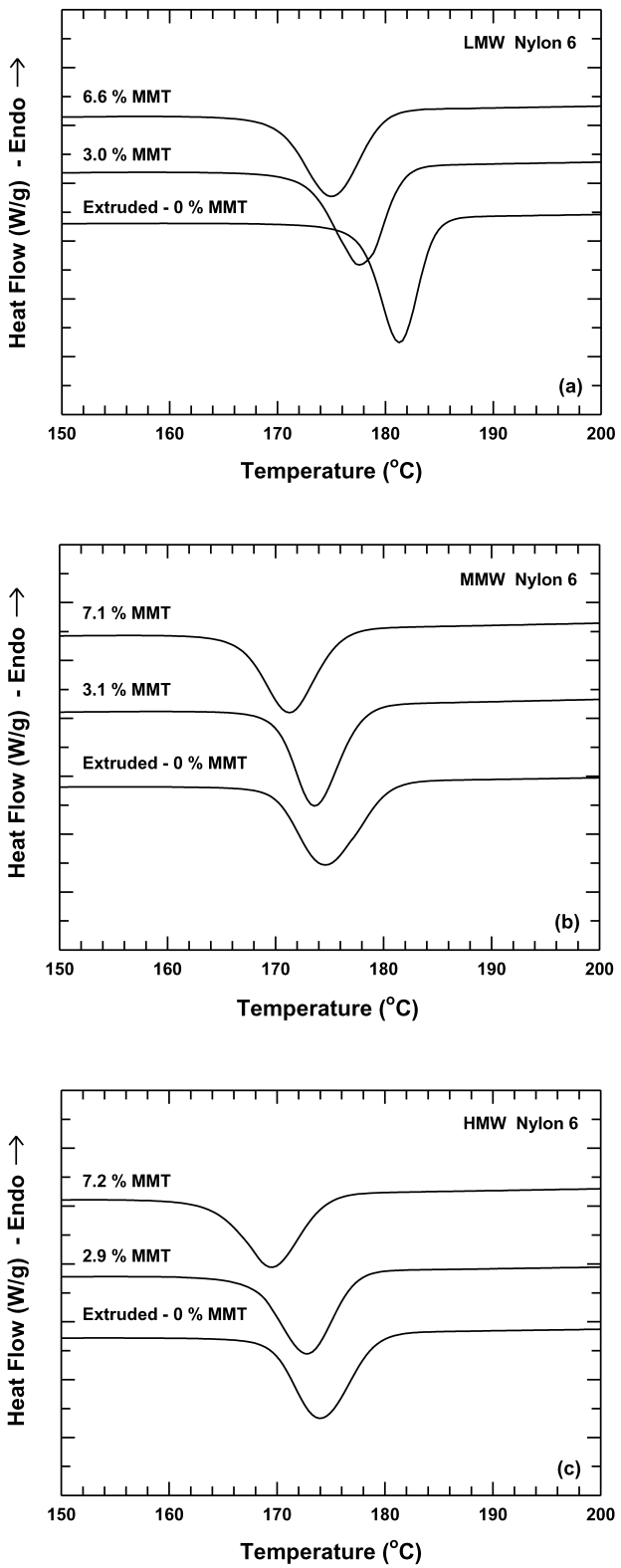

Fig. 9. Cooling scans of samples taken from extruded nylon 6 and its nanocomposites based (a) LMW, (b) MMW, and (c) HMW nylon 6. Samples were obtained from pellets that were dried under vacuum for 12 h at 80 °C prior to DSC analysis. Samples were held at 250 °C for 1 min prior to cooling at 20 °C/min. Scans are shifted for clarity.

Table 3
Differential scanning calorimetry data for extruded pellets of nylon 6 nanocomposites based on $(HE)_2M_1R_1$ organoclay under non-isothermal heating and cooling conditions

Polymer sample	% MMT	First heating		Cooling		Second heating		
		T_m [a] (°C)	x_c [b] (%)	T_{cc} (°C)	ΔH_c [c] (J/g)	T_g (°C)	T_m [a] (°C)	x_c [b] (%)
LMW-virgin	0.0	208.7/220.4	26.4	176.9	75	51.7	209.2/219.1	31.0
MMW-virgin	0.0	219.1	46.6	160.1	61.8	51	219.4	27.6
HMW-virgin	0.0	218.7	45.8	158.6	55.2	51.1	211.8/218.7	24.9
LMW-extruded	0.0	215.1/219.4	28.5	181.3	77.5	51.1	208.7/218.4	32.5
LMW	3.0	206.9/219.1	27.4	177.6	78.4	49.7	210.0/217.4	32.1
LMW	6.6	207.9/218	26.0	174.9	75	49.5	211.3/218.4	31.6
MMW-extruded	0.0	209/219.1	27.5	174.6	71.8	49.9	208.4/218.1	30.5
MMW	3.1	207.9/218.7	26.0	173.6	72.6	50.4	211.3/218.4	29.0
MMW	7.1	209.2/217.5	25.7	171.3	70	51.3	211.6/217.4	28.0
HMW-extruded	0.0	208.5/218.7	25.2	173.8	68.8	50.5	209.5/218.1	29.1
HMW	2.9	208.1/218.4	25.3	172.9	68.1	51.7	211.6/217.1	26.8
HMW	7.2	208.7/217.6	25.1	169.6	68.5	50.6	211.3/216.7	27.2

Samples were held for 2 min at −10 °C, heated from −10 to 250 °C at 20 °C/min, held for 1 min at 250 °C, cooled from 250 to −10 °C at 20 °C/min, held for 2 min at −10 °C, and subsequently heated from −10 to 250 °C at 20 °C/min.

[a] Values in italics represent minor low temperature endotherms.

[b] x_c is calculated by the ratio of $\Delta H_m/\Delta H_m^\circ$ where ΔH_m° is the average of ΔH_m° (α) and ΔH_m° (γ) listed in Table 1, i.e. 240 J/g.

[c] ΔH values are based on the amount of pure polyamide within the composite sample.

of the fibers [80–84]; therefore, core-skin effects must be considered when designing injection molded parts.

Fig. 10 shows DSC melting endotherms of samples taken from the core and skin regions of injection molded specimens; Table 4 summarizes data from such scans. The endotherms presented in Fig. 10 permit the examination the effects of MMT concentration, polyamide molecular weight, and sample location, i.e. core versus skin. The scans in Fig. 10(a–c), from the core region of injection molded specimens, show the result of adding dispersed montmorillonite on melting is three fold regardless of the polyamide matrix molecular weight. First, low temperature endothermic peaks around 208 °C are introduced with addition of clay; the height and breadth of these peaks increases, at the expense of the major peak, with increasing clay content. Second, the peak temperature of the main endotherm slightly decreases with increasing clay content. Third, the onset of melting occurs at slightly lower temperatures for the nanocomposites. Increasing the clay concentration results in a minor decrease in percent crystallinity as seen in Table 4.

The above observations may arise from a variety of factors; the formation of a small shoulder prior to the endothermic peak may be associated with the γ crystalline form of nylon 6 as suggested by various researchers [46,54,85]. Aharoni advocates that the lower melting point of the γ-form is due to the lower crystalline density and increased entropy of melting associated with the reduction in trans-conformation bonding as compared to the α counterpart [16]. Although this reasoning seems plausible, the presence of low temperature melting peaks as well as broadening effects may simply reflect changes in crystallite thickness

Table 4
Differential scanning calorimetry data for injection molded samples of nylon 6 nanocomposites based on $(HE)_2M_1R_1$ organoclay under non-isothermal heating and cooling conditions

Polymer matrix	Sample location	% MMT	Heating		
			T_m [a] (°C)	ΔH_m [b] (J/g)	x_c [c] (%)
LMW	Core	0.0	218.4	79.3	33.0
LMW	Skin	0.0	212.0/220.1	66	27.5
LMW	Core	3.0	207.4/218.1	71.9	30.0
LMW	Skin	3.0	217.7	75.3	31.4
LMW	Core	6.6	207.9/217.4	69.8	29.1
LMW	Skin	6.6	217.4	75.0	31.3
MMW	Core	0.0	219.4	74.6	31.1
MMW	Skin	0.0	216.4/220.7	71	29.6
MMW	Core	3.1	208.2/218.7	70.5	29.4
MMW	Skin	3.1	218.4	77.3	32.2
MMW	Core	7.1	208.2/217.1	64.3	26.8
MMW	Skin	7.1	217.1	70.8	29.5
HMW	Core	0.0	220.1	68.3	28.4
HMW	Skin	0.0	219.4	67	27.9
HMW	Core	2.9	208.5/217.7	65.5	27.3
HMW	Skin	2.9	218.1	68.0	28.3
HMW	Core	7.2	207.7/217.1	58.4	24.4
HMW	Skin	7.2	216.7	59.6	24.9

Samples were held for 2 min at −10 °C, heated from −10 to 250 °C at 20 °C/min, held for 1 min at 250 °C, and then subsequently cooled from 250 to −10 °C at 20 °C/min.

[a] Values in italics represent minor low temperature endotherms.

[b] ΔH_f values are based on the amount of pure polyamide within the composite sample.

[c] x_c is calculated by the ratio of $\Delta H_m/\Delta H_m^\circ$ where ΔH_m° is the average of ΔH_m° (α) and ΔH_m° (γ) listed in Table 1, i.e. 240 J/g.

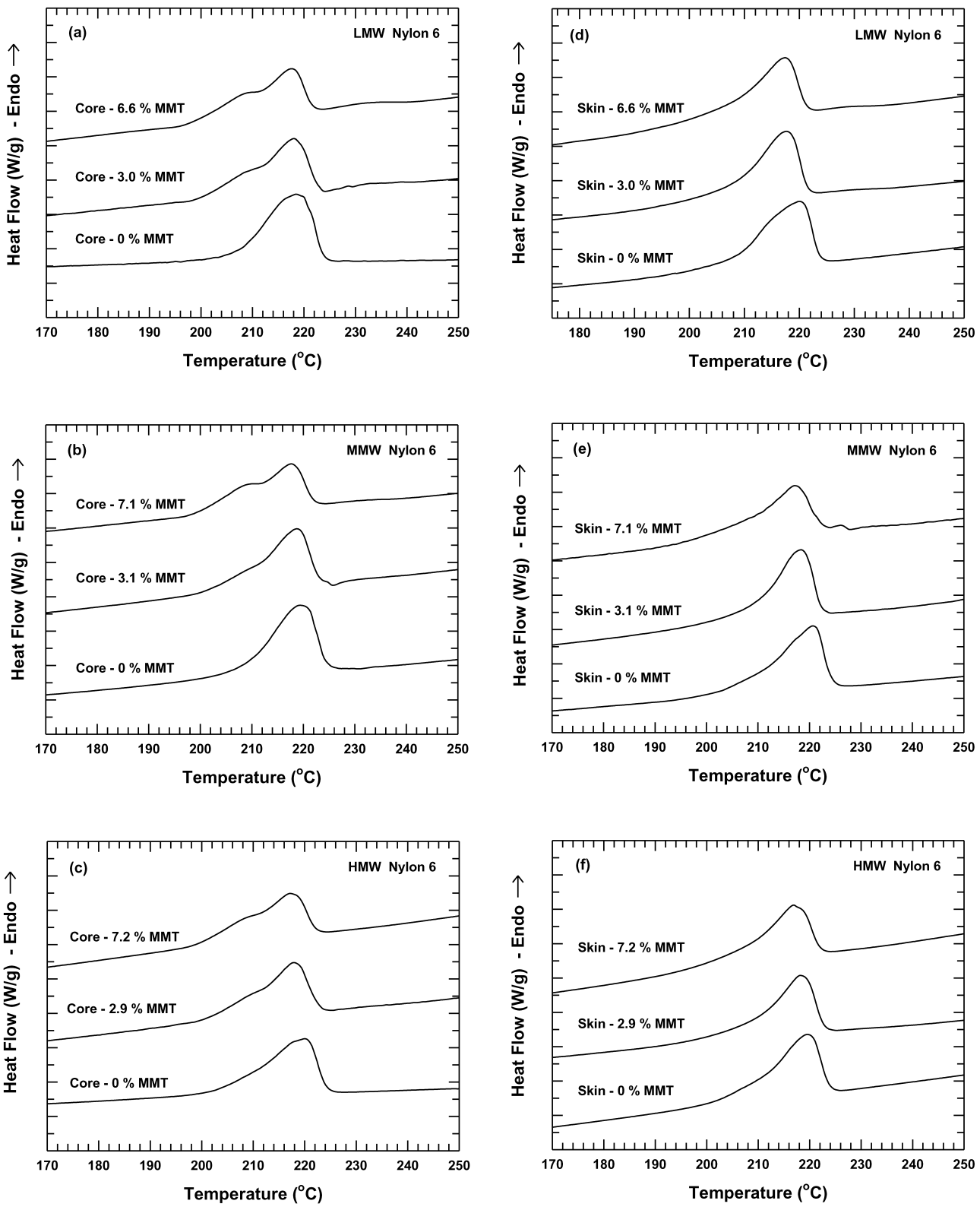

Fig. 10. Heating scans of samples taken from the core (a–c) and skin (d–f) of injection molded bars made from extruded nylon 6 and its nanocomposites based on LMW, MMW, and HMW nylon 6. Samples were heated at a rate of 20 °C/min. Scans are shifted for clarity.

and its distribution. The lower crystallinity seen in the nanocomposite is due to the inability of polymers chains to be fully incorporated into growing crystalline lamella. In other words, the presence of high concentrations of dispersed MMT platelets prevents large crystalline domains from forming due to limited space and restrictions imposed on polymer chains by a high number of silicate platelets; this leads to smaller crystallite structures and more defect ridden crystalline lamella. Lincoln et al. showed by SAXS experiments on nylon 6 nanocomposites that clay layers do indeed disrupt crystallite formation and, in turn, lead to less ordered crystals [8]. Such imperfections in crystalline structure may also explain the lower melting points observed for the nanocomposites.

WAXD data presented in Fig. 11(a–c) and Table 5 help clarify hypotheses made in the analysis of DSC thermograms. All samples contain peaks at $2\theta \cong 20$ and 23.7°, corresponding to the α_1 and α_2 peaks of the α-form, and 21.3° indicative of the γ-form. Similar behavior in nylon 6 nanocomposites has been observed by Varlot et al. and Devaux et al. [86,87]. Increasing the level of MMT does not significantly alter the relative proportions of the α and γ-forms in the core region; this leads to the conclusion that the low temperature endotherms observed in the DSC heating scans are more likely associated with decreases in crystallite lamella thickness. Interestingly, adding clay leads to no clear trend in the level of core crystallinity (see Table 5). This may reflect limitations in the peak deconvolution method used to estimate the level of crystallinity. Therefore, at this point it is important to comment on the limitations of using X-ray methods, as well as DSC methods, for evaluating degree of crystallinity.

A number of complications are involved in estimating crystallinity from WAXD data [88]. First, X-ray scattering from semi-crystalline polymers consists of a superposition of crystalline and amorphous patterns. Separation of the two parts is often somewhat subjective, particularly when more than one crystalline reflection exists. Second, diffuse scattering from defects in the crystal cannot be distinguished from the amorphous halo. Third, subtraction of the baseline may remove portions of both crystalline and amorphous scattering. Lastly, scanning in only one azimuthal direction may be insufficient for injection molded specimens. Complete rotation of the sample along three principle directions will better describe the crystalline structure.

Errors are also inherent in the determination of crystallinity via DSC. For example, accurate values of ΔH_f° must be known; this is further complicated when two crystalline forms are present, as in nylon 6. Changes in crystalline structure, e.g. cold crystallization, melting, stress relaxation, and moisture related effects can occur upon heating which further complicates DSC thermograms and subsequent analysis, as pointed out by Khanna and Kuhn [89]. Finally, care must be taken when constructing a baseline for calculating ΔH_f. Based on these points, the level of crystallinity reported by each technique has its limitations that should be remembered when comparing data.

There is little influence of matrix molecular weight on the peak melting temperature in the core region for the nanocomposites. Although, the pure polyamide samples show a slight increase in peak temperature with respect to molecular weight, T_m is approximately the same for the three types of nylon 6 nanocomposites. The higher T_m for the unfilled MMW and HMW nylon 6 may be a result of more ordered crystallites, e.g. fewer chain ends lead to better chain folding and packing. The level of crystallinity in the core obtained by DSC (see Table 4), however, does exhibit a substantial decrease with increasing molecular weight for pure nylon 6 and its nanocomposites. The decrease is attributed to the polymer matrix and not the filler since the level of decrease is approximately the same regardless of the filler concentration. X-ray scans of the core also show that increasing the molecular weight increases the level of the α-form.

Heating scans of skin samples in Fig. 10(d–f) reveal different relationships with regard to clay concentration and

Table 5
Crystallinity data obtained from theoretical fitting of wide angle X-ray patterns obtained on injection molded specimens of nylon 6 nanocomposites based on $(HE)_2M_1R_1$ organoclay

Polymer matrix	% MMT	Core				Skin			
		% α	% γ	Total (%)	% γ of Total	% α	% γ	Total (%)	% γ of Total
LMW	0.0	11	19	30	63	0	16	16	100
LMW	3.0	9	20	30	68	0	46	46	100
LMW	6.6	12	17	30	59	0	51	51	100
MMW	0.0	21	9	30	30	0	13	13	100
MMW	3.1	22	7	29	24	0	49	49	100
MMW	7.1	22	3	25	12	0	40	40	100
HMW	0.0	22	10	32	31	0	17	17	100
HMW	2.9	32	5	37	14	0	42	42	100
HMW	7.2	28	10	38	26	0	45	45	100

WAXD intensity—2θ patterns were fitted using the profile fitting program PeakFit™ (AISN Software Inc.) with a Gaussian–Lorentzian peak shape.

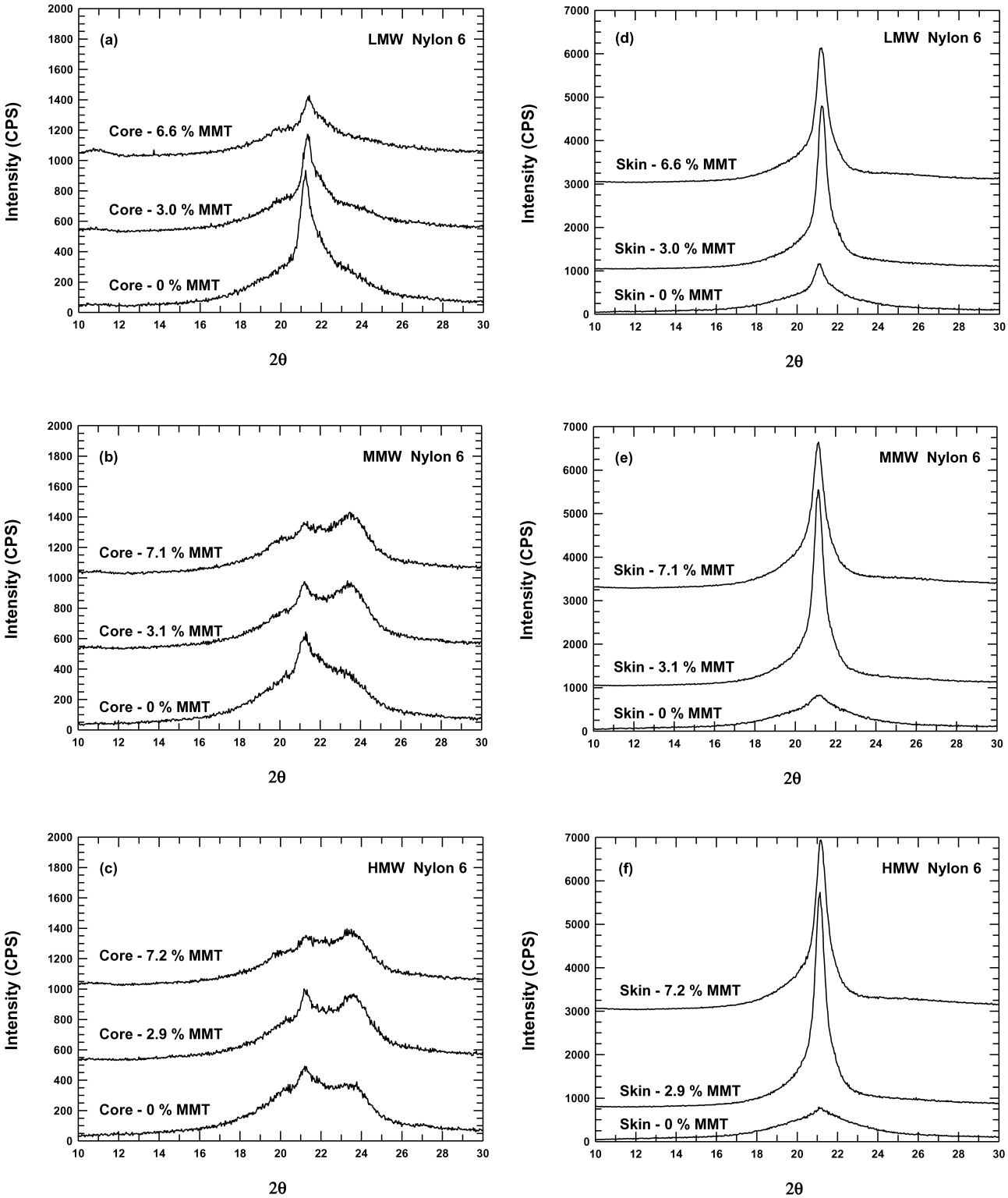

Fig. 11. WAXD profiles obtained from (a–c) core and (d–f) skin region of injection molded bars made from nylon 6 and nanocomposites based on LMW, MMW, and HMW nylon 6. Scans are shifted for clarity.

polyamide molecule weight. Adding dispersed clay does not produce an additional endothermic peak as in the core samples. However, the breadth of the peaks increases while their temperature location slightly decreases with increasing MMT concentration. The most pronounced disparity between core and skin is seen in the level of crystallinity, x_c. Adding clay results in an increase in x_c for the skin, yet a decrease for the core samples. Also, crystallinity is

consistently higher for the skin, except for the pure polyamide where the opposite is true. Before attempting to explain this trend, it is best to examine the WAXD data of the skin samples presented in Fig. 11(–f) and Table 5.

The skin X-ray patterns in Fig. 11, unlike the respective core scans, consist only of the γ-crystalline form. This probably reflects the higher cooling rates (hence lower crystallization temperatures) and the high levels of stress in the skin than the core. Adding dispersed clay to the skin region enhances the amount of γ; this is evident in the more intense peaks seen in Fig. 11(–f). Interestingly, the intermediate concentration of MMT has the highest X-ray intensity for each polyamide molecular weight, yet each peak is sharper, e.g. smaller full-width at half-height, than nanocomposites with higher clay contents; this likely denotes more ordered, larger crystallites due to fewer polymer-silicate interactions in the samples of intermediate clay contents. X-ray scans of the skin also show that increasing the molecular weight increases the intensity of the γ-peak; this may stem from the higher levels of clay platelet exfoliation in the MMW and HMW matrices [7,12,13]. The crystallinity values of the skin presented in Table 5 are higher for nanocomposites than their respective matrixes. Moreover, the skin has consistently higher levels of crystallinity than the core for the nanocomposite, while the opposite is true for the pure polyamides [7,12,13]. This trend qualitatively mimics the observation made in x_c values obtained by DCS. Similar observations were reported by Akkapedi [90,91] on injection molded samples.

The trends observed for the percent crystallinity and the proportion of α and γ-forms are the result of several issues. From the literature, it is expected that rapid cooling of nylon 6 from the melt favors the formation of γ-crystals. Rapid cooling forces crystallization to occur at low temperatures where the rate is limited by polymer chain mobility; mobility limitations may be the cause for favoring the γ-form. Slow cooling, on the other hand, allows crystallization to occur at higher temperatures where the rate is mainly dominated by the driving force or degree of undercooling. The latter conditions favor the formation of the α-form. The above WAXD results show that injection molded samples contain the γ-form in the skin region and a mixture of α and γ-forms in the core region; this can be explained by the differences in cooling rates or subsequently crystallization temperatures that each region experiences; i.e. heat transfer causes rapid cooling in the skin and slower cooling in the core. Introducing dispersed clay in the molded nylon 6 appears to modify the structure of the skin, where γ conditions prevail; however, this has little effect in the core, where α conditions are present. Therefore, the clay platelets seem to only effect the crystal structure under γ-favored conditions; this is likely why higher levels of crystallinity are observed in the skin than the in the core for the nanocomposites. Furthermore, if limitations in chain mobility indeed promote crystallization into the γ-form, then adding clay platelets will further decrease chain mobility and increase the likelihood of γ-crystal production. Lastly, it is unclear what role stress plays in the differences in crystallinity seen within these materials. The high surface area clay platelets are capable of high degrees of alignment in injection molding, as shown previously [10]. The additional stresses imposed on the polymer chains by clay surfaces may further align polymer chains, especially in the skin region where stresses are the highest; thus facilitating crystal formation.

5. Conclusions

Investigations on polymer crystallization behavior and crystal morphology were carried out on nylon 6 nanocomposites formed by melt processing. Isothermal and non-isothermal crystallization experiments were used to evaluate the influence of clay concentration, polyamide molecular weight, and the degree of clay platelet exfoliation on the kinetics of polymer crystal formation. These studies show that crystallization kinetics of the nanocomposites are dramatically increased at very low filler concentrations relative to extruded polyamide matrices; however, higher clay loadings retard the crystallization process. Nanocomposites containing commercially relevant concentrations of clay, i.e. ~3–5 wt%, have comparable crystallization times and temperatures as the pure polyamide with a similar processing history. In general, crystallization rates are enhanced more for nanocomposites formed from high molecular weight polyamides, most likely due to better platelet exfoliation, which provides more filler surface for crystal nucleation [72].

Morphological studies by X-ray diffraction and DSC revealed significant differences in crystal type and quantity within the skin and core regions of injection molded nanocomposites. The skin region contains only the γ-crystalline form; this is largely due to the rapid cooling of the skin to low temperatures and possibly limited polymer chain mobility. Increasing the concentration of clay within the skin enhances the formation of the γ-form, which may be related to further restrictions in polymer chain mobility. The core region, on the other hand, contains both the α and γ-forms of nylon 6. Interestingly, higher levels of crystallinity were observed in the skin than in the core for the nanocomposites, while the opposite is true for the pure polyamides. Based on these results, it appears that the clay primarily affects the nylon 6 crystal structure under γ-favored conditions, i.e. rapid cooling, mobility restricted conditions, and/or high strain. Future studies in this laboratory will attempt to address differences in mechanical properties between these two forms.

Acknowledgements

This work was funded by the Air Force Office of

Scientific Research. The authors would like to thank Fabien Lansade of the Grenoble Institute of Science and Technology and Randy Chapman of Southern Clay Products for their assistance with DSC and WAXD analysis.

References

[1] Fujiwara S, Sakamoto T. Japan, Patent No. JP-A-51-109998; 1976 (assigned to Unitika Ltd., Japan).
[2] Okada A, Fukushima Y, Kawasumi M, Inagaki S, Usuki A, Sugiyami S, Kurauchi T, Kamigaito O. United States, Patent No. 4739007; 1988 (assigned to Toyota Motor Co., Japan).
[3] Usuki A, Kojima Y, Kawasumi M, Okada A, Fukushima Y, Kurauchi T, Kamigaito O. J Mater Res 1993;8(5):1179–84.
[4] Christiani BR, Maxfield M. United States, Patent No. 5747560; 1998 (assigned to Allied Signal).
[5] Liu L, Qi Z, Zhu X. J Appl Polym Sci 1999;71(7):1133–8.
[6] Cho JW, Paul DR. Polymer 2001;42(3):1083–94.
[7] Fornes TD, Yoon PJ, Hunter DL, Keskkula H, Paul DR. Polymer 2002;43(22):5915–33.
[8] Lincoln DM, Vaia RA, Wang Z-G, Hsiao BS. Polymer 2001;42(4): 1621–31.
[9] Dennis HR, Hunter DL, Chang D, Kim S, White JL, Cho JW, Paul DR. Polymer 2001;42(23):9513–22.
[10] Yoon PJ, Fornes TD, Paul DR. Polymer 2002;43(25):6727–41.
[11] Krishnamoorti R, Giannelis EP. Macromolecules 1997;30(14): 4097–102.
[12] Fornes TD, Yoon PJ, Keskkula H, Paul DR. Polymer 2001;42(25): 09929–40.
[13] Fornes TD, Yoon PJ, Keskkula H, Paul DR. Polymer 2002;43(7): 2121–2.
[14] Kojima Y, Usuki A, Kawasumi M, Okada A, Fukushima Y, Kurauchi T, Kamigaito O. J Mater Res 1993;8(5):1185–9.
[15] Ito M, Mizuochi K, Kanamoto T. Polymer 1998;39(19):4593–8.
[16] Aharoni SM. n-Nylons, their synthesis, structure, and properties. Chichester; New York: Wiley; 1997.
[17] Arimoto H, Ishibashi M, Hirai M, Chatani Y. J Polymer Sci Pt A 1965; 3(1):317–26.
[18] Holmes DR, Bunn CW, Smith DJ. J Polymer Sci 1955;17:159–77.
[19] Kohen MI, editor. Nylon plastics handbook. New York: Hanser; 1995.
[20] Murthy NS. Polym Commun 1991;32(10):301–5.
[21] Rybnikar F, Burda J. Faserforsch u Textiltech 1961;12:324–31.
[22] Roldan LG, Kaufman HS. Polym Lett 1960;1:603–8.
[23] Itoh T, Miyaji H, Asai K. Jpn J Appl Phys 1975;14(2):206–15.
[24] Reichle A, Prietzschk A. Angew Chem 1962;74:562–9.
[25] Wallner LG. Monatsh 1948;79:279–95.
[26] Illers KH, Haberkorn H, Simak P. Makromol Chem 1972;158: 285–311.
[27] Illers KH. Makromol Chem 1978;179(2):497–507.
[28] Illers KH, Haberkorn H. Makromol Chem 1971;142:31–67.
[29] Gogolewski S, Gasiorek M, Czerniawska K, Pennings AJ. Colloid Polym Sci 1982;260(9):859–63.
[30] Vogelsong DC. J Polymer Sci 1963;1(Pt. A):1055–68.
[31] Rybnikar F. Chem listy 1958;52:1042–8.
[32] Marx P, Smith CW, Worthington AE, Dole M. J Phys Chem 1955;59: 1015–9.
[33] Dole M, Wunderlich B. Makromol Chem 1959;34:29–49.
[34] Inoue M. J Polymer Sci Pt A 1963;1:2013–20.
[35] Starkweather Jr. HW, Zoller P, Jones GA. J Polym Sci, Polym Phys Ed 1984;22(9):1615–21.
[36] Wunderlich B, Macromolecular physics, vol. 3. New York: Academic Press; 1973.
[37] Fornes TD. Polyamide-Layered Silicate Nanocomposites by Melt Processing. PhD Dissertation. University of Texas at Austin, Chem Eng; 2003.
[38] Gurato G, Fichera A, Grandi FZ, Zannetti R, Canal P. Makromol Chem 1974;175(3):953–75.
[39] Kyotani M, Mitsuhashi S. J Polym Sci, Part A-2 1972;10(8): 1497–508.
[40] Brill R. J Prakt Chem 1942;161:49–64.
[41] Murthy NS, Aharoni SM, Szollosi AB. J Polym Sci, Polym Phys Ed 1985;23(12):2549–65.
[42] Murthy NS, Curran SA, Aharoni SM, Minor H. Macromolecules 1991;24(11):3215–20.
[43] Ramesh C, Gowd EB. Macromolecules 2001;34(10):3308–13.
[44] Lincoln DM, Vaia RA, Wang ZG, Hsiao BS, Krishnamoorti R. Polymer 2001;42(25):09975–85.
[45] Salem DR, Moore RAF, Weigmann HD. J Polym Sci, Part B: Polym Phys 1987;25(3):567–89.
[46] Campoy I, Gomez MA, Marco C. Polymer 1998;39(25):6279–88.
[47] Okada A, Kawasumi M, Tajima I, Kurauchi T, Kamigaito O. J Appl Polym Sci 1989;37(5):1363–71.
[48] Magill JH. Polymer 1962;3:655–64.
[49] Wu Q, Liu X, Berglund LA. Macromol Rapid Comm 2001;22(17): 1438–40.
[50] Liu X, Wu Q. Euro Polym Journal 2002;38(7):1383–9.
[51] Wu Q, Liu X, Berglund LA. Polymer 2002;43(8):2445–9.
[52] Liu X, Wu Q. Polymer 2002;43(6):1933–6.
[53] Wu T-M, Liao C-S. Macromol Chem Phys 2000;201(18):2820–5.
[54] Wu T-M, Chen E-C, Liao C-S. Polym Eng Sci 2002;42(6):1141–50.
[55] VanderHart DL, Asano A, Gilman JW. Chem Mater 2001;13(10): 3796–809.
[56] VanderHart DL, Asano A, Gilman JW. Chem Mater 2001;13(10): 3781–95.
[57] Khanna YP, Kumar R, Reimschuessel AC. Polym Eng Sci 1988; 28(24):1607–11.
[58] Khanna YP, Reimschuessel AC, Banerjie A, Altman C. Polym Eng Sci 1988;28(24):1600–6.
[59] Khanna YP, Kumar R, Reimschuessel AC. Polym Eng Sci 1988; 28(24):1612–5.
[60] Khanna YP, Reimschuessel AC. J Appl Polym Sci 1988;35(8): 2259–68.
[61] Khanna YP. Polym Eng Sci 1990;30(24):1615–9.
[62] Avramova N. Polym Polym Compos 1993;1(4):261–74.
[63] Magill JH. Polymer 1962;3(No. 1):43–51.
[64] Turska E, Gogolewski S. Polymer 1971;12(10):616–28.
[65] Turska E, Goglewski S. J Appl Polym Sci 1975;19(3):637–44.
[66] Avramova N, Fakirov S, Avramov I. J Polym Sci, Polym Phys 1984; 22(2):311–3.
[67] Avramova N, Fakirov S. J Polym Sci, Polym Phys 1986;24(4):761–8.
[68] Fornes TD, Yoon PJ, Paul DR. Manuscript in preparation.
[69] Jimenez G, Ogata N, Kawai H, Ogihara T. J Appl Polym Sci 1997; 64(11):2211–20.
[70] Ma J, Zhang S, Qi Z, Li G, Hu Y. J Appl Polym Sci 2002;83(9): 1978–85.
[71] Wunderlich B, Macromolecular physics, vol. 2. New York: Academic Press; 1973.
[72] Gurato G, Gaidano D, Zannetti R. Makromol Chem 1978;179(1): 231–45.
[73] Mudra I, Balazs G. J Therm Anal Calorim 1998;52(2):355–61.
[74] Avrami A. J Chem Phys 1939;7:1103.
[75] Avrami A. J Chem Phys 1940;8:212.
[76] Avrami A. J Chem Phys 1941;9:177.
[77] Turska E, Gogolewski S. Polymer 1971;12(10):629–41.
[78] Khanna YP, Taylor TJ. Polym Eng Sci 1988;28(16):1042–5.
[79] Tadmor Z, Gogos CG. Principles of polymer processing. SPE monographs. New York: Wiley; 1979.
[80] Laura DM, Keskkula H, Barlow JW, Paul DR. Polymer 2000;41(19): 7165–74.

[81] Friedrich K. Plast Rubber Process Appl 1983;3(3):255–65.
[82] Karger-Kocsis J, Friedrich K. Compos Sci Technol 1988;32(4): 293–325.
[83] Karger-Kocsis J, Friedrich K. Plast Rubber Process Appl 1989;12(1): 63–8.
[84] Karger-Kocsis J, Friedrich K. Int J Fatigue 1989;11(3):161–8.
[85] Liu X, Wu Q. Polymer 2002;43(6):1933–6.
[86] Varlot K, Reynaud E, Kloppfer MH, Vigier G, Varlet J. J Polym Sci, Part B: Polym Phys 2001;39(12):1360–70.
[87] Devaux E, Bourbigot S, El Achari A. J Appl Polym Sci 2002;86(10): 2416–23.
[88] Runt JP. In: Kroschwitz JI,, editors, 2nd ed. Encyclopedia of polymer science and engineering, vol. 4. New York: Wiley; 1985. p. 482–519.
[89] Khanna YP, Kuhn WP. J Polym Sci, Part B: Polym Phys 1997;35(14): 2219–31.
[90] Akkapeddi MK. Proceedings of 57th Annu Tech Conf—Soc Plast Engng, vol. 2; 1999. p. 1619–22.
[91] Akkapeddi MK. Polym Compos 2000;21(4):576–85.